Research Article Wiley Online Library ELECTROANALYSIS

doi.org/10.1002/elan.202100198

Multi-Walled Carbon Nanotubes and Gold Nanorod Decorated Biosensor for Detection of microRNA-126

Seda Nur Topkaya,*[a] Ezgi Turunc,[b] and Arif E. Cetin[c]

Abstract: In this article, we introduced a novel electrochemical biosensor for the detection of microRNA-126. The biosensor utilizes a hybridization assay combined with multi-walled carbon nanotubes and gold nanorod-decorated screen-printed carbon electrodes. For electrode preparation, gold nanorods were first immobilized onto the surface of bare and multi-walled carbon nanotube-modified screen-printed carbon electrodes, and the thiol tagged-capture probe was immobilized on the electrode surface through gold and thiol group interaction. After the immobilization, thiol tagged-capture probe hybridized with the target sequence. Under optimum conditions, we determined limit of detection (LOD) and limit of quantification (LOQ) as high as 11 nM and 36 nM, respectively.

Keywords: Electrochemical Biosensor · mir-126 · Voltammetry · Multi-walled Carbon Nanotubes · Gold Nanorods

1 Introduction

MicroRNA (miRNA) is a single stranded, short (18–24 nucleotides) and non-protein encoding RNA, which involves in numerous biological processes. They play key regulatory roles, e.g., cell differentiation, stress response, proliferation, and apoptosis [1]. They could be used as a biomarker especially in liquid biopsy due to their minimally invasive nature. They are also stable in the blood stream and resistant to fragmentation by either enzymatic or chemical agents [2]. However, detection of miRNA is challenging due to the short size of oligonucleotides, sequence similarities, and their low amount in biological samples. Therefore, a sensitive, selective, rapid and affordable method is needed for the detection of miRNAs in clinic for diagnosis and prognosis [3]. In literature, different platforms have been developed that utilize expensive and time-consuming traditional techniques, and require challenging sample preparation protocols, e.g., northern blot [4], reverse transcription polymerase chain reaction (RT-PCR) [5], microarrays, [6] and RNA sequencing [7]. New technologies have been also developed for the detection of miRNA, e.g., DNA machine, synthetic molecular machinery based on programmed sequence-specific interactions of DNA strands [8], and CRISPR/Cas13a powered portable electrochemiluminescence [9].

Strategies relying on biosensors such as electrochemical, colorimetric, optical, mass sensitive, and electrochemiluminescent platforms employing nanomaterials or enzymatic signal amplification have been offered as a strong candidate over the traditional methods as they could provide rapid and sensitive responses, exhibit a non-toxic nature, and possess simple experimental steps. Among those, electrochemical biosensors are promising due to their advantages, e.g., simple instrumentation and stable operation. Carbon derivate nanomaterials, e.g., carbon nanotubes (CNTs), carbon nanofibers, graphene, graphene oxide (GO) nano-sheets, and gold nanoparticles, provide electro-conductivity, large effective surface area and biocompatibility [10]. Particularly, single- (SWCNTs) and multi-walled carbon nanotubes (MWCNTs) are preferred for biosensing applications as they could provide low limit-of-detections [11]. MWCNTs functionalized with nanomaterials could also provide new physical or chemical modalities to biosensors [12].

As a promising nanomaterial, gold nanorods (AuNRs) have been widely used in biosensing applications for diagnostic, imaging and therapeutic applications. Rod-shaped nanostructures have one-dimensional structure that provides excellent electrocatalytic properties and strong electron transfer platforms. They could be manufactured in different aspect ratios, which could alter their optical properties [13]. Moreover, they have high stability and could be prepared with self-assembly techniques [13a].

Among gold-based morphologies, e.g., cage or sphere, AuNRs have the highest surface cross-section with higher efficiency of cell adhering [14]. Furthermore, they ensure low agglomeration at the immobilization surface due to their shape, and are compatible for biomolecule immobilization. More importantly, AuNRs have an easy-to-adjust

[a] S. N. Topkaya
Department of Analytical Chemistry, Faculty of Pharmacy, Izmir Katip Celebi University, Cigli 35620, Izmir, Turkey
E-mail: sedanur6@gmail.com
sedanur.topkaya@ikcu.edu.tr
[b] E. Turunc
Department of Biochemistry, Faculty of Pharmacy, Izmir Katip Celebi University, Cigli 35620, Izmir, Turkey
[c] A. E. Cetin
Izmir Biomedicine and Genome Center, Balcova 35340, Izmir, Turkey

nature using thiol-ended molecules. Recently, gold nanoparticles combined with CNTs have been used to create nano-hybrid materials exhibiting new properties, which could be critical for wide range of applications, e.g., sensors [15], biosensors [16], and drug delivery [17]. Moreover, MWCNTs could provide reliable support to stabilize nanometer-sized gold particles, which yields ultra-sensitive detection of biological molecules.

mir-126, a member of miRNA family, has critical roles in cellular biology, e.g., cancer biology, inflammation, vascular development, and angiogenesis. It plays an important role in atherosclerosis, coronary artery disease, stroke, and diabetic vasculopathy, and is used as a biomarker for cardiovascular diseases [18]. Downregulation of mir-126 expression generally occurs in vascular diseases [19]. Moreover, mir-126 has also an important function in diseases related to brain and retina. As an important biomarker candidate and a therapeutic target for vascular diseases and cancer, detection of mir-126 is very critical.

In literature, there are numerous miRNA detection strategies, e.g., Au nanoparticle decorated-reduced graphene oxide (GO) nanocomposites via streptavidin-alkaline-phosphatase catalyzed assay [20], thiolated probe-functionalized gold nanorods and GO oxide for miRNA-155 via an intercalating label Oracet Blue [21],, an impidimetric method using biotinylated polythiophene film coated gold SPE for miR-221 [22], and SWCNT-grafted dendritic Au nanostructure on fluorine-doped tin oxide electrode for miR-21 [23]. Furthermore, electrochemical biosensors are available that employ either MWCNTs or AuNRs, while their combination has not been investigated for the detection of mir-126.

To our knowledge, combination of AuNRs and MWCNTs with SPEs has not been reported for the detection of mir-126 yet. In this article we, for the first time, developed a label-free electrochemical biosensor for mir-126 detection via hybridization with the use of AuNRs/MWCNTs modified screen-printed carbon electrodes (SPEs). We investigated the electrochemical behavior of AuNRs/MWCNTs modified SPEs (AuNRs/MWCNTs/SPEs) through differential pulse voltammetry (DPV), cyclic voltammetry (CV), and electrochemical impedance spectroscopy (EIS), and explored their functionality by comparing their electrochemical properties with those of bare SPEs and MWCNTs modified SPEs (MWCNT/SPEs). We evaluated probe-target hybridization by monitoring changes within the guanine oxidation current, where the decrease in this current was used as an indicator for mir-126 hybridization. Synergistic effect of AuNRs and MWCNTs showed an excellent electrocatalytic activity and a convenient surface for mir-126 hybridization. Voltammetry and impedance-based electrochemical methods were, for the first time, used to realize sequence-specific detection of mir-126. Specificity of the mir-126 biosensor was evaluated with the use of non-complementary sequences. Under optimum conditions, the platform yields a limit of detection (LOD) and limit of quantification (LOQ), 11 nM and 36 nM, respectively. Our biosensor supports excellent stability over 8 weeks, longer than the stability data in literature, which is an important asset for commercial applications requiring long storage period.

2 Experimental

2.1 Chemicals, Oligonucleotides, and Electrodes

Gold Nanorods: CTAB capped bare gold nanorods (A12-10-750-CTAB-25) with 10-nm-diameter and 35-nm-length (Nanopartz, USA) were purified in DI-water with trace CTAB, and used in the experiments without any modification. To prevent aggregation of AuNRs, stock solutions were sonicated for 10 s before each experiment.

Oligonucleotides: Synthetic oligonucleotides in HPLC purified-lyophilized powder format (Eurofins Genomics, Germany) were used without purification. Stock solutions of oligonucleotides were prepared with water for injection. Diluted solutions of probe were prepared in 0.5 M Acetate Buffer (pH: 4.8, ACB), while those of target and non-complementary sequences were prepared in 0.05 M Phosphate Buffer (pH 7.4, PBS). In this article, specific mir-126 RNA sequences were labelled as target. Sequences complementary to target (antimir-126) were labelled as probe, which functions as bio-recognition element. Non-complementary oligonucleotides (mir-21), possessing different sequences compared to target, were used as control to determine the specificity of our biosensor.

Synthetic oligonucleotide sequences are shown below:

Probe

Probe antimir-126: 5'-CGC ATT ATT ACT CAC GGT ACG A-3'

–SH tagged Probe antimir-126: 5'-SH CGC ATT ATT ACT CAC GGT ACG A-3'

–NH_2 tagged Probe antimir-126: 5'-NH_2 CGC ATT ATT ACT CAC GGT ACG A-3'

Target

mir-126 (RNA): 5'-UCG UAC CGU GAG UAA UAA UGC G-3'

Non-Complementary (Control)

NC-1 (mir-21 (DNA)): 5'-TAG CTT ATC AGA CTG ATG TTG A-3'

NC-2 (mir-21 (RNA)): 5'- UAG CUU AUC AGA CUG AUG UUG A-3'

Electrodes: SPEs (ref. DRP-110) and MWCNT/SPEs (ref. DRP-110CNT) were received from DropSens, Metrohm (Spain).

2.2 Method

2.2.1 Characterization of AuNRs

The morphology of AuNRs was investigated with a scanning electron microscope (SEM, Hitachi S-4800, Japan). AuNRs were characterized with a UV-Vis spectrophotometer (Shimadzu UV-3600, Japan), where its absorbance spectra were recorded between 400 to 1000 nm.

2.2.2 Label-Free Electrochemical Detection of mir-126

2.2.2.1 Activation of Bare SPEs and MWCNT/SPEs

SPEs were first rinsed with 50 % ethanol and DI-water to eliminate impurities. In order to obtain steady voltammograms, bare SPEs and MWCNT/SPEs were electrochemically activated through 10 potential cycles between +0.5 V and +1.8 V with a scan rate of 100 mV/s in PBS [24].

2.2.2.2 Preparation and Immobilization of AuNRs onto Bare SPEs and MWCNT/SPEs

AuNRs were diluted by a factor of 20 with PBS. For the modification of AuNRs at the surface of bare SPEs and MWCNT/SPEs, 50 µL AuNRs solution was dropped onto the activated bare SPEs and MWCNT/SPEs, where it was incubated for 2 h, and rinsed with PBS afterwards.

2.2.2.3 Detection of mir-126 via Hybridization

The steps for the detection of mir-126 are shown in Figure 1.

Antimir-126 Probe Immobilization: Dilute solutions of –SH tagged antimir-126 probe (–SH Probe) was daily prepared with PBS. 50 µL –SH Probe solution with 5 µg/mL concentration was immobilized onto AuNRs/MWCNT/SPEs for 1 h, which forms a gold-thiol (Au–SH) bond. Probe coated electrodes were rinsed with PBS to remove unbound –SH Probe from the surface. Following this step, 50 µL 6-mercapto-1-hexanol (6-MCH) with 1 mM concentration prepared in PBS was immobilized for 1 h. 6-MCH was used for efficient hybridization by block-

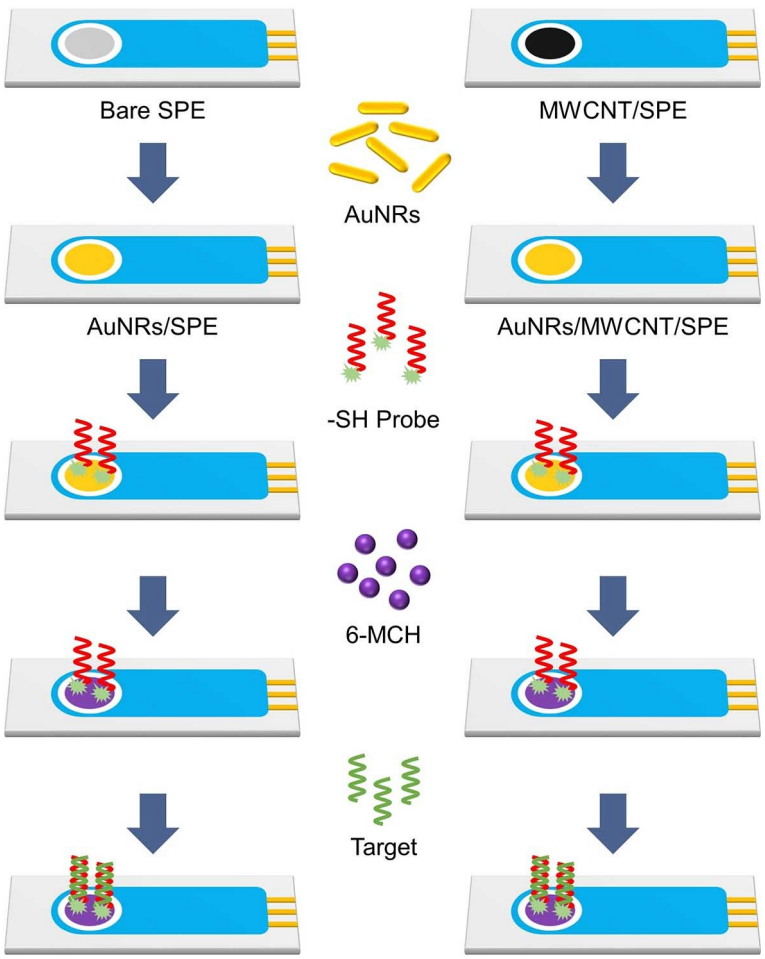

Fig. 1. Schematic illustration for the electrochemical detection of mir-126.

ing unreacted gold surface, and eliminating non-specific adsorption. In the last step, electrodes were rinsed with PBS.

Solid-Phase Hybridization with mir-126: Dilute solutions of mir-126 were daily prepared with PBS. Probe-target hybridization was realized through 1 h immobilization of 50 µL mir-126 target solution. Target solutions were prepared by dissolving different concentrations of target in the hybridization solution. In the last step, electrodes were rinsed with PBS. To determine the specificity of our biosensor, non-complementary sequences, e.g., mir-21 DNA and mir-21 RNA, were used as control evaluated under the same hybridization conditions.

2.2.2.4 Electrochemical Measurement

DPV, CV, and EIS were carried out with a Potentiostat/Galvanostat/Impedance Analyzer (Metrohm, AUTOLAB 204.FRA32 M model with NOVA 2.1 software). All DPV measurements were performed in ACB from +0.4 V to +1.4 V at 100 mV/s scan rate with 0.5 s interval time. CV and EIS measurements were performed in 10 mM $K_3(Fe(CN)_6/K_4(Fe(CN)_6$ solution. CV scan rate was between 20–200 mV/s.

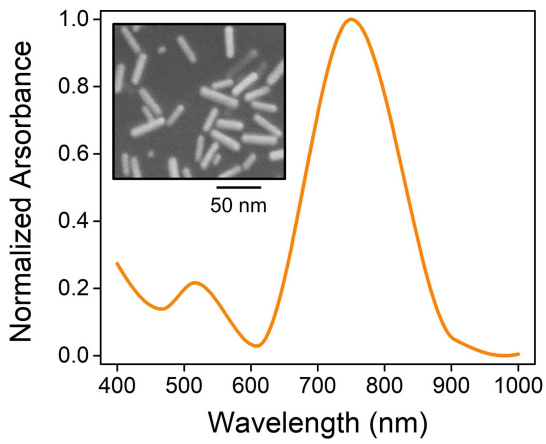

Fig. 2. UV-Vis absorption spectrum and SEM image (inset) of AuNRs.

3 Results and Discussion

3.1 Characterization of AuNRs

We investigated the morphological properties of AuNRs via UV-Vis spectrometry and scanning electron microscopy. Figure 2 shows the UV-Vis absorption spectrum and the SEM image (inset) of AuNRs. For UV measurements, 100 µL AuNRs solution was filled into a cuvette, and the absorption spectrum was measured at a 0.5 nm sampling interval with single scan mode. As shown in Figure 2, the absorption peak of AuNRs was obtained at ~750 nm, which is associated with the localized surface plasmon excitations. SEM image shows that nanorods are not aggregated, and have uniform shapes. The diameter of AuNRs is ~35 nm.

3.2 Activation Effect of Bare SPEs and MWCNT/SPEs

Electrochemical [25] or mechanical [26] activation of SPEs enhances voltammetric responses, and increases sensitivity. Activation step is also crucial for the stability of electrochemical biosensors, e.g., due to insufficient activation, nanomaterials or biological molecules could detach from the surface, which results in instability of the biosensors. Mechanical activation is realized by polishing SPEs with either commonly available alumina slurry or diamond spray. In general, electrochemical activation is more preferred than mechanic activation. Activation is critical as SPEs are electrochemically less active due to their polymeric material restricting electron transfer reaction at the electrode-electrolyte interface, which decreases electron transfer. Thus, SPEs are electrochemically activated to improve edge planes [24]. In electrochemical activation, repetitive voltammetric cycles are applied at a certain potential.

In Figure 3, we compared electrochemical response of activated and non-activated bare SPEs and MWCNT/

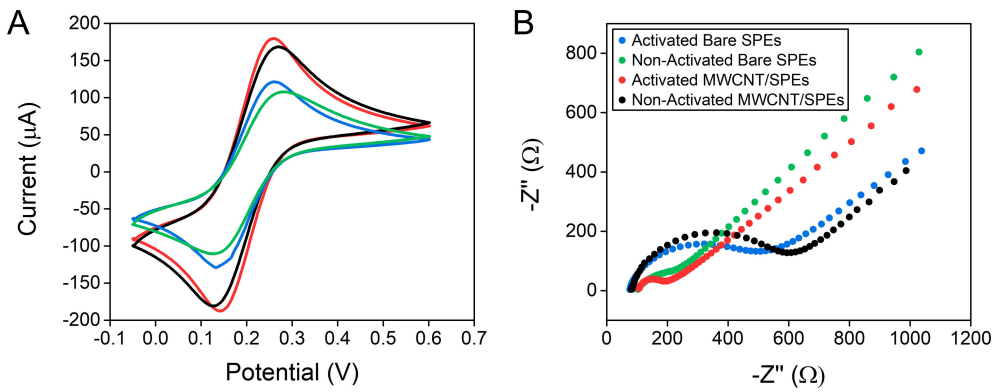

Fig. 3. **(A)** CV and **(B)** EIS spectra of activated and non-activated bare SPEs (blue, green) and MWCNT/SPEs (red, black) in 10 mM $K_3(Fe(CN)_6/K_4(Fe(CN)_6$ solution. Figures are color-coded.

SPEs through CV and EIS (blue/green: activated/non-activated bare SPEs, red/black: activated/non-activated MWCNT/SPEs). In experiments, bare SPEs and MWCNT/SPEs were electrochemically activated in PBS with CV, e.g., between +0.5 V and +1.8 V for 10 cycles at a scan rate of 100 mV/s. Their electrochemical responses were evaluated with CV and EIS in 10 mM $K_3(Fe(CN)_6/K_4(Fe(CN)_6$ solution. In Figure 3A, CV spectrum has different electrochemical behaviors for activated and non-activated bare SPEs and MWCNT/SPEs. For both MWCNT/SPEs and SPEs, current dramatically increased after the activation, while higher currents were obtained for MWCNT/SPEs compared to bare SPEs due to MWCNTs' ability to increase electrode active surface area. For both SPEs, activation dramatically increased the peak currents, which is attributed to the acceleration of electron transfer.

We performed EIS experiments to confirm CV results. As shown in Figure 3B, non-activated SPEs showed a large semicircle, which suggests a very high electron transfer resistance compared to other electrodes. Activated SPEs exhibit smaller charge transfer resistance (R_{ct}) compared to non-activated SPEs. A significant decrease in R_{ct} was observed for MWCNT/SPEs unlike bare SPEs, which implies MWCNTs' good electrical conductivity that could accelerate electron transfer of the electrochemical probe.

3.3 Comparison of SPEs, MWCNT/SPEs and AuNRs/MWCNT/SPEs

Carbon nanotubes have negatively charged surfaces due to functional oxide surface groups, e.g., carboxylic and hydroxyl groups, which are widely used as electrode material in electroanalytical chemistry. Combination of MWCNTs with gold particles provides unique properties, e.g., strong activity, higher electrocatalytic activity and stability. In our work, SPEs and MWCNT/SPEs were commercially supplied, and electrochemically activated. In order to demonstrate the function of AuNRs in our biosensor system, we deposited AuNRs onto bare SPEs and MWCNT/SPEs via passive adsorption. AuNRs could easily enter inside the network, and locate stably on the electrode surface due to the porous structure of the carbon membrane [27].

Figure 4A shows the CV spectrum of bare SPEs (blue), MWCNT/SPEs (red), and AuNRs/MWCNT/SPEs (orange) in a 10 mM $K_3(Fe(CN)_6/K_4(Fe(CN)_6$ solution, showing that AuNRs/MWCNT/SPEs yield the highest catalytic activity. For example, AuNRs/MWCNT/SPEs shows higher redox peak currents compared to bare SPEs and MWCNTs/SPEs. The electrochemically active surface area of the modified electrode was calculated with Randles-Sevcik Equation 1.

$$Ip = 2.72.10^5\ n^{3/2}\ A\ D^{1/2}\ C\ \upsilon^{1/2} \quad (1)$$

In Equation 1, I_p is the peak current, n is the number of electrons involved in the redox reaction, υ is the scan rate (Vs^{-1}), A is the electrochemical active area (cm^2), D is the diffusion coefficient ($cm^2\,s^{-1}$), and C is the concentration of $[Fe(CN)_6]^{3-/4-}$ ($mol\,cm^{-3}$). According to Equation 1, active surface areas were calculated as 0.9 ± 0.04, 1.6 ± 0.08, and 9.0 ± 0.1 mm^2 for bare SPEs, MWCNT/SPEs, and AuNRs/MWCNT/SPEs, respectively. Electroactive surface area of AuNRs/MWCNT/SPEs increased ~10 fold compared to bare SPES, demonstrating its better conductivity desired for sensing applications. To our knowledge, our biosensor has more active surface area compared to the earlier study reported in literature [28].

Nanoparticle-modified working electrodes have three unique advantages over their unmodified counterparts, e.g., enhancement of mass transport, catalysis, and high effective surface area [29]. Nanoparticles enable higher rate of mass transport to the electrode surface such that the peak current determined for the nanoparticle-modified and -unmodified electrodes could be differentiated. On the other hand, catalytic properties of nanoparticles could cause a decrease in the overpotential, and allow higher peak-to-peak separation (ΔE_p). As shown in Figure 4A, ΔE_p is lower for AuNRs/MWCNT/SPEs com-

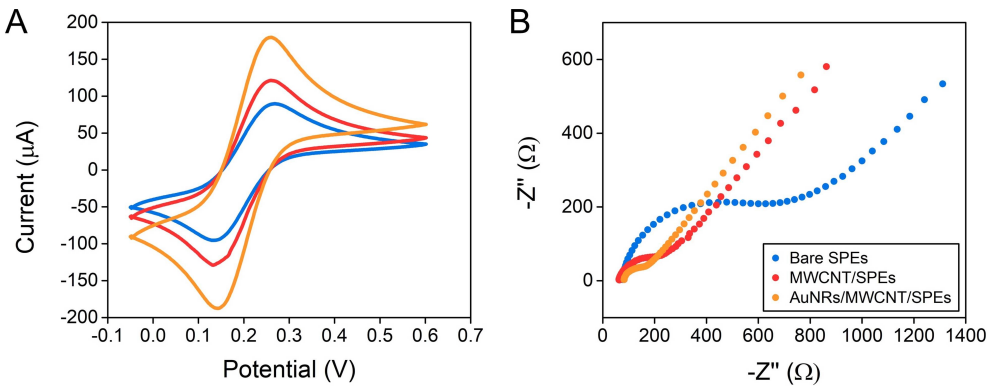

Fig. 4. **(A)** CV and **(B)** EIS spectrum of bare SPEs, (blue) MWCNT/SPEs (red), and AuNRs/MWCNT/SPEs (orange) in 10 mM $K_3(Fe(CN)_6/K_4(Fe(CN)_6$ solution. Figures are color-coded.

pared to MWCNT/SPEs and bare SPEs, which indicates the rapid electron transfer on the modified electrodes, e.g., AuNRs/MWCNT/SPEs > MWCNT/SPEs > bare SPEs.

Figure 4B shows the Nyquist plots determined by EIS. After the modification of AuNRs on MWCNT/SPEs, R_{ct} dramatically decreased, e.g., by 72 %, compared to bare SPEs and MWCNT/SPEs. Therefore, AuNRs-modified SPEs is more sensitive to variations in the electrons on the surface compared to bare SPEs and MWCNT/SPEs. Here, we determined the R_{ct} values as $435 \pm 8\ \Omega$, $123 \pm 5\ \Omega$, and $65 \pm 4\ \Omega$ for bare SPEs, MWCNT/SPEs and AuNRs/MWCNT/SPEs, respectively. In the Nyquist plot, AuNRs/MWCNT/SPEs shows a small diameter, which suggests a fast electron-transfer rate and low R_{ct}. This is due to the strong conductivity of MWCNTs and AuNRs that arises from their synergistic effect. Here, both bare SPEs and MWCNT/SPEs become more conductive to improve the electron transfer between electrolytic solution and the electrode in the presence of AuNRs [27]. AuNRs have good electrical properties, and could improve active surface and electron transfer rate, i.e., they could be integrated to biosensor systems.

3.4 Detection of mir-126

In the previous section, we determined the optimum parameters for the highest sensing signal related to AuNRs/MWCNT/SPEs. In this section, we determined the proper probe for effective immobilization. Accordingly, we immobilized different types of probes onto the electrode surface, and performed CV and EIS tests. CV measurements were performed to investigate probe effect on redox signal (Figure 5A). Here, the peak current determined for bare AuNRs/MWCNT/SPEs (orange) is highest compared to probe coated electrodes. Peak current decreased after modification for all probe types, which suggests that non-conductive probe binding on the electrode surface could act as a barrier making interfacial charge transfer inaccessible. Coating electrodes with probe could also hinder electron transfer on the electrode surface. The highest decrease in current was obtained with –SH Probe (purple) due to the specific and strong interaction between Au–SH group of the probe. Redox currents of Probe (black) and $–NH_2$ Probe (gray) coated electrodes are very close to bare electrodes which demonstrates that there is no effective interaction between Au and these probes.

Figure 5B shows the Nyquist plots for bare AuNRs/MWCNT/SPEs (orange), Probe (black), $-NH_2$ Probe (gray), and –SH Probe (purple) coated AuNRs/MWCNT/SPEs in 10 mM $K_3(Fe(CN)_6/K_4(Fe(CN)_6$ solution. Compared to bare electrodes, R_{ct} values increased with Probe, –SH Probe, and $-NH_2$ Probe coated AuNRs/MWCNT/SPEs. The highest resistance was determined for –SH Probe coated AuNRs/MWCNT/SPEs due to the electron transfer blocking in $K_3(Fe(CN)_6/K_4(Fe(CN)_6$. This could be attributed to the decline in the electron transfer ability for $K_3(Fe(CN)_6/K_4(Fe(CN)_6$ as a result of the probe oligonucleotide deposition. After the interaction between AuNRs and –SH Probe, R_{ct} value increased by ~2.2 fold compared to bare AuNRs/MWCNT/SPEs, which indicates their strong interaction.

This increase in R_{ct} could be attributed to the insulation effect of the phage layers onto the surface of the electrodes. As Au possess a strong interaction with –SH groups, more biomolecules, (e.g., thiol terminated capture probe) immobilized at the electrode surface. Consistency between CV and EIS characterization indicates that probe immobilization ensures effective hybridization.

One important step for a successful hybridization is the immobilization efficiency of the capture probe. Therefore, we explored the effect of probe concentration and immobilization time on the analytical performance of our biosensor via DPV (Figure 6). Electro-activity of guanine bases could be used for direct measurement of nucleic acids in label-free assays [30]. We investigated the effect of probe concentration on biosensor performance by monitoring guanine oxidation current in Figure 6A. To find the optimum probe concentration, –SH Probe in the range between 1 and 20 µg/mL was immobilized onto

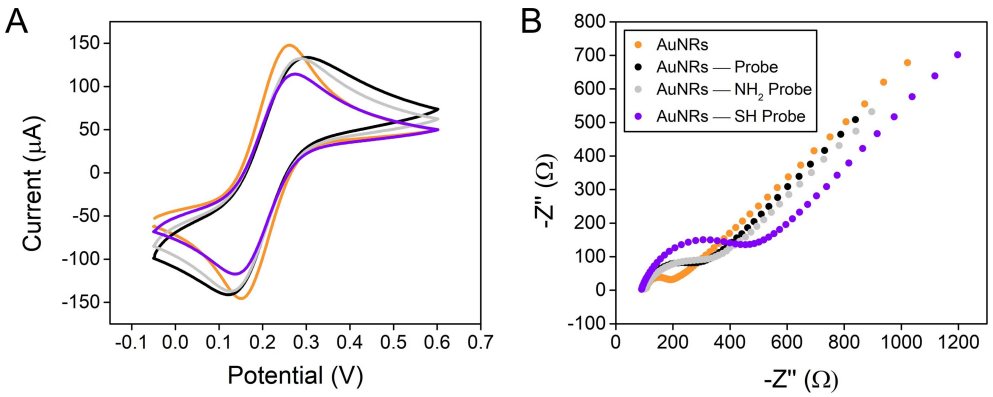

Fig. 5. **(A)** CV and **(B)** EIS spectrum of bare AuNRs/MWCNT/SPEs (orange), Probe (black), $-NH_2$ Probe (gray), and –SH Probe (purple) coated AuNRs/MWCNT/SPEs in 10 mM $K_3(Fe(CN)_6/K_4(Fe(CN)_6$ solution. Figures are color-coded.

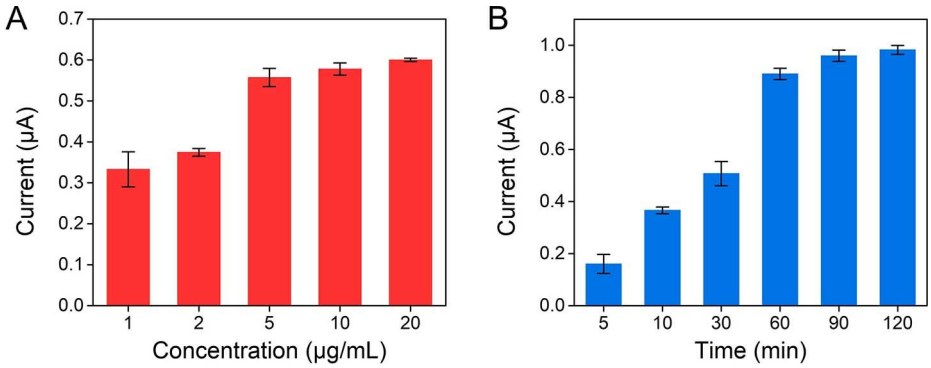

Fig. 6. Histograms of guanine oxidation signals for **(A)** probe concentration and **(B)** probe immobilization time. Error bars denote standard deviation of five independent experiments.

AuNRs/MWCNT/SPEs. After probe immobilization, electrodes were rinsed with PBS to remove unbound probe followed by the voltammetric measurements. In the voltammetric measurements, we observed a gradual increase in current with probe concentration until 5 μg/mL, which is the saturation level, e.g., chosen as the optimum probe concentration. As shown in the next section, surface of AuNRs/MWCNT/SPEs was saturated via –SH Probe, which eliminates non-specific binding of target mir-126 to provide the best hybridization efficiency. Figure 6B shows the histogram of guanine oxidation current as a function of probe immobilization time from 5 to 120 min. Here, we observed that guanine oxidation current increased with time and remained almost unchanged after 60 min. Therefore, for the hybridization studies, probe immobilization time was chosen as 60 min.

Hybridization between complementary sequences, e.g., probe and target, is the most preferred biorecognition scheme compared to enzymes or antibodies due to their strong stability and short assay time. In order to find the optimum target concentration, we formed various hybrids between antimir-126 and mir-126 while changing the target concentration at a fixed probe concentration. In DPV analyses, guanine oxidation currents were evaluated before and after hybridization. Figure 7A shows that, amplitude of the guanine oxidation current for hybrid significantly decreases with target concentration until 5 μg/mL (blue: probe, red: target). Figure 7B shows the calibration curve determined from ΔCurrent ($\Delta I = I_{PROBE} - I_{HYBRID}$) vs. logarithm of miRNA-126 concentration. Linear regression equation was found as $\Delta I = 276.59 \times \log(\text{Target Concentration}) + 117.64$, where $R^2 = 0.9941$. For mir-126 detection, we used the formulation as, e.g., limit of detection, LOD = (3 × SD)/(Slope of Calibration Curve), and limit of quantification, LOQ = (10 × SD)/(Slope of Calibration Curve), where SD is the standard deviation calculated by regression analysis for S/N = 3. Under optimum conditions, LOD and LOQ were calculated as 11 nM and 36 nM, respectively.

We investigated the ability of our platform to form solid-phase hybridization via DPV, where guanine oxidation currents were measured before and after hybridization. As shown in Figure 7C, guanine oxidation current of probe (blue) is higher than those of hybrid (red) since oxidation is more difficult in a hybrid structure compared to probe. The reason is that the electron transfer from the inside of the hybrid RNA to the electrode surface is more challenging compared to flexible probe RNA, which leads to higher peak currents in the probe. Our results demonstrated that a complementary target could pair with the probe, which leads a significant decrease in the guanine oxidation current due to hybridization. We performed control experiments to evaluate the selectivity of the biosensor, where two non-complementary sequences for mir-126 (NC1: orange, NC2: green) were used as target. We observed no change in the guanine oxidation current for NC1 and NC2, which proves our biosensor's selectivity to target mir-126. Finally, we performed EIS measurements to evaluate hybridization, where Nyquist plots were determined for probe (blue), hybrid (red), NC1 (orange), and NC2 (green) immobilized on AuNRs/MWCNT/SPEs. Figure 7D shows that R_{ct} calculated for probe increased upon the immobilization of target, NC1, and NC2. Increase in R_{ct} for hybrid is the result of the accumulation of negatively charged phosphate backbone of mir-126 on the probe coated electrodes. However, R_{ct} values for NC1 and NC2 were not as resistive as hybrid, which proves the absence of hybridization between probe and non-complementary sequences.

3.5 Stability of mir-126 Biosensor

In order to evaluate the stability of our biosensor, –SH Probe coated electrodes were stored at +4 °C for different storage durations in weeks. The electrodes were then hybridized with target mir-126, and analyzed with the protocol explained in Section 2.2.2.4. As shown in Table 1, we observed no significant change in the peak current until week 8, which demonstrates our biosensor's strong stability. This stability duration is longer than previously reported data in literature for miRNA detection [31]. Providing long shelf life, our cost-effective and disposable biosensor could be a good candidate for commercial use for mir-126 detection.

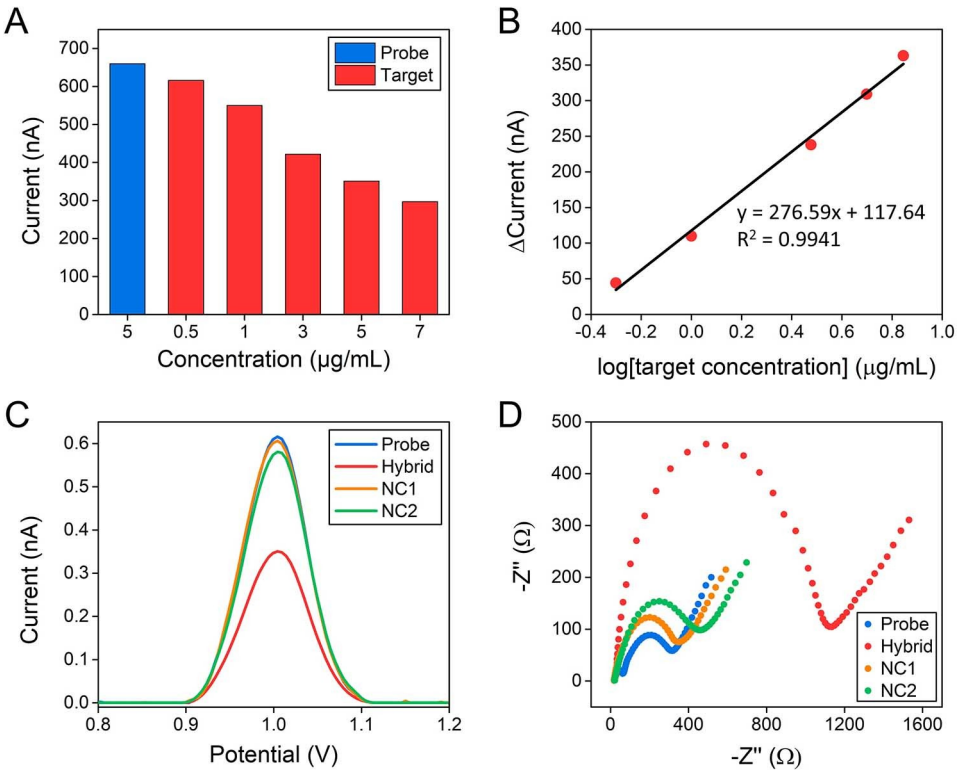

Fig. 7. **(A)** Histogram and **(B)** calibration curve of the hybridization study using different target concentrations: 0.5, 1, 3, 5, 7 µg/mL at constant probe concentration, 5 µg/mL. **(C)** DPV and **(D)** EIS of probe, hybrid, NC-1, and NC-2.

Table 1. Stability of mir-126 biosensor for different storage durations at +4 °C (n = 5).

Storage Duration at +4 °C (weeks)	Average response of the mir-126	RSD Value (%)
0	100	2.4
1	98.4	2.1
2	96.5	4.8
3	94.2	6.5
4	93.7	5.8
8	85.6	8.8
12	74.3	12.5
16	60.2	13.3

4 Conclusion

miRNA detection often requires amplification, labeling, or radioactive probes. The detection could be achieved in either spiked human serum, cell lines, or tissues. The disadvantage of a tissue-based detection is the need for invasive procedures, e.g., biopsy. In our study, we successfully detected mir-126, and selectively discriminated it from control sequences in synesthetic samples. In this article, we developed a sensitive, selective, and robust electrochemical RNA biosensor platform with the use of AuNRs/MWCNT/SPEs for the detection of mir-126. Electrostatic interaction between negatively charged MWCNTs surface and positively charged AuNRs surface stabilized the electrode material, and provided a functionalized surface for a sensitive detection. AuNRs/MWCNT/SPEs displayed stronger catalytic activity and lower redox potentials compared to bare electrodes. We used CV and EIS analyses to investigate electrochemical properties of modified SPEs. We showed that electroactive surface area of MWCNT/AuNRs/SPEs increased by ~10 folds compared to bare SPEs. We determined LOD and LOQ of the biosensor as 11 nM and 36 nM, respectively with a signal-to-noise ratio of 3. In our biosensor platform, such a high sensitivity was achieved by combining an excellent electrical conductivity of multi-walled carbon nanotubes and gold nanorods. Providing rapid, sensitive and selective sensing data, our electrochemical platform is promising for point-of-care detection of mir-126. Moving from the proof-of-concept detection of synthetic mir-126 sequences, we will test our detection assay with real patient samples prepared from serum in the future.

Acknowledgement

This work was financially supported by Izmir Katip Celebi University (Project No: 2018-GAP-ECZF-0002).

Data Availability Statement

Data available on request from the authors.

References

[1] L. F. R. Gebert, I. J. MacRae, *Nat. Rev. Mol. Cell Biol.* **2019**, *20*, 21–37.

[2] P. S. Mitchell, R. K. Parkin, E. M. Kroh, B. R. Fritz, S. K. Wyman, E. L. Pogosova-Agadjanyan, A. Peterson, J. Noteboom, K. C. O'Briant, A. Allen, D. W. Lin, N. Urban, C. W. Drescher, B. S. Knudsen, D. L. Stirewalt, R. Gentleman, R. L. Vessella, P. S. Nelson, D. B. Martin, M. Tewari, *Proc. Natl. Acad. Sci. USA* **2008**, *105*, 10513–10518.

[3] P. S. Sfragano, S. Pillozzi, I. Palchetti, *Electrochem. Commun.* **2021**, *124*, 106929.

[4] M. Schwarzkopf, N. A. Pierce, *Nucleic Acids Res.* **2016**, *44*, e129.

[5] H. Zhang, X. Zou, L. Wu, S. Zhang, T. Wang, P. Liu, W. Zhu, J. Zhu, *Cancer Med.* **2020**, *9*, 1230–1241.

[6] W. Yuan, L. Liu, L. Liang, K. Huang, Y. Deng, M. Dong, J. Chen, G. Wang, F. Zou, *Gene* **2020**, *724*, 144156.

[7] Y. Ibuki, Y. Nishiyama, Y. Tsutani, M. Emi, Y. Hamai, M. Okada, H. Tahara, *PLoS One* **2020**, *15*, e0231116.

[8] P. Miao, Y. Tang, *Small* **2020**, *16*, e2004518.

[9] T. Zhou, R. Huang, M. Huang, J. Shen, Y. Shan, D. Xing, *Adv. Sci.* **2020**, *7*, 1903661.

[10] a) J. Mohanraj, D. Durgalakshmi, R. A. Rakkesh, S. Balakumar, S. Rajendran, H. Karimi-Maleh, *J. Colloid Interface Sci.* **2020**, *566*, 463–472; b) F. Wang, Y. Chu, Y. Ai, L. Chen, F. Gao, *Mikrochim. Acta* **2019**, *186*, 116; c) K. C. Lin, S. Muthukumar, S. Prasad, *Talanta* **2020**, *214*, 120810; d) P. Kanagavalli, M. Veerapandian, *Biosens. Bioelectron.* **2020**, *150*, 111878.

[11] a) Z. Zhao, J. Zheng, E. P. Nguyen, D. Tao, J. Cheng, H. Pan, L. Zhang, N. Jaffrezic-Renault, Z. Guo, *Mikrochim. Acta* **2020**, *187*, 500; b) F. Hu, W. Zhang, W. Meng, Y. Ma, X. Zhang, Y. Xu, P. Wang, Y. Gu, *Anal. Chim. Acta* **2020**, *1109*, 9–18; c) H. Li, S. Ding, W. Wang, Q. Lv, Z. Wang, H. Bai, Q. Zhang, *Mikrochim. Acta* **2019**, *186*, 860.

[12] a) M. Rouhani, A. Soleymanpour, *Mikrochim. Acta* **2020**, *187*, 512; b) A. Guner, E. Cevik, M. Senel, L. Alpsoy, *Food Chem.* **2017**, *229*, 358–365.

[13] a) R. A. Taheri, Y. Akhtari, T. Tohidi Moghadam, B. Ranjbar, *Sci. Rep.* **2018**, *8*, 9333; b) M. Mazaheri, A. Simchi, H. Aashuri, *Mikrochim. Acta* **2018**, *185*, 178; c) Y. Zhang, T. Jiang, L. Tang, *Biosens. Bioelectron.* **2017**, *97*, 278–284.

[14] N. Gong, S. Chen, S. Jin, J. Zhang, P. C. Wang, X.-J. Liang, *Regen. Biomater.* **2015**, *2*, 273–280.

[15] V. Mani, T. S. T. Balamurugan, S. T. Huang, *Int. J. Mol. Sci.* **2020**, *21*, 2853.

[16] a) M. Amatatongchai, W. Sroysee, S. Chairam, D. Nacapricha, *Talanta* **2015**, *133*, 134–141; b) S. Han, W. Liu, M. Zheng, R. Wang, *Anal. Chem.* **2020**, *92*, 4780–4787.

[17] Y. Shu, Q. Lu, F. Yuan, Q. Tao, D. Jin, H. Yao, Q. Xu, X. Hu, *ACS Appl. Mater. Interfaces* **2020**, *12*, 49480–49488.

[18] a) L. Miao, R. X. Yin, Q. H. Zhang, X. J. Hu, F. Huang, W. X. Chen, X. L. Cao, J. Z. Wu, *Nutr. Metab.* **2019**, *16*, 39; b) X. Fu, T. Niu, X. Li, *Front. Neurosci.* **2019**, *13*, 866; c) J. Liu, J. Liu, L. Shi, F. Zhang, L. Yu, X. Yang, J. Cai, *Int. J. Mol. Med.* **2018**, *41*, 1835–1844.

[19] B. Yu, Y. Jiang, X. Wang, S. Wang, *Med. Res. Arch.* **2020**, *8*.

[20] C. Ingrosso, M. Corricelli, F. Bettazzi, E. Konstantinidou, G. V. Bianco, N. Depalo, M. Striccoli, A. Agostiano, M. L. Curri, I. Palchetti, *J. Mater. Chem. B* **2019**, *7*, 768–777.

[21] M. Azimzadeh, M. Rahaie, N. Nasirizadeh, K. Ashtari, H. Naderi-Manesh, *Biosens. Bioelectron.* **2016**, *77*, 99–106.

[22] D. Voccia, M. Sosnowska, F. Bettazzi, G. Roscigno, E. Fratini, V. De Franciscis, G. Condorelli, R. Chitta, F. D'Souza, W. Kutner, I. Palchetti, *Biosens. Bioelectron.* **2017**, *87*, 1012–1019.

[23] A. Sabahi, R. Salahandish, A. Ghaffarinejad, E. Omidinia, *Talanta* **2020**, *209*, 120595.

[24] P. Sundaresan, T. W. Chen, S. M. Chen, T. W. Tseng, X. Liu, *Int. J. Electrochem. Sci.* **2018**, *13*, 1441–1451.

[25] a) M. I. González-Sánchez, B. Gómez-Monedero, J. Agrisuelas, J. Iniesta, E. Valero, *Electrochem. Commun.* **2018**, *91*, 36–40; b) R. d O Silva, É. A. da Silva, A. R. Fiorucci, V. S. Ferreira, *J. Electroanal. Chem.* **2019**, *835*, 220–226.

[26] a) L. R. Cumba, C. W. Foster, D. A. C. Brownson, J. P. Smith, J. Iniesta, B. Thakur, D. R. do Carmo, C. E. Banks, *Analyst* **2016**, *141*, 2791–2799; b) J. Lee, D. W. M. Arrigan, D. S. Silvester, *Anal. Chem.* **2016**, *88*, 5104–5111.

[27] Q. K. Vu, Q. H. Tran, N. P. Vu, T.-L. Anh, T. T. L. Dang, T. Matteo, T. H. H. Nguyen, *Mater. Today Commun.* **2020**, *26*, 101726.

[28] a) M. Govindasamy, S. Manavalan, S.-M. Chen, U. Rajaji, T.-W. Chen, F. M. A. Al-Hemaid, M. A. Ali, M. S. Elshikh, *J. Electrochem. Soc.* **2018**, *165*, B370–B377; b) L. Bai, R. Yuan, Y. Chai, Y. Yuan, Y. Wang, S. Xie, *Chem. Commun.* **2012**, *48*, 10972–10974.

[29] F. W. Campbell, R. G. Compton, *Anal. Bioanal. Chem.* **2010**, *396*, 241–259.

[30] a) S. N. Topkaya, A. E. Cetin, *Electroanalysis* **2020**, *32*, 112–118; b) S. N. Topkaya, A. E. Cetin, *Electroanalysis* **2019**, *31*, 1554–1561; c) S. N. Topkaya, *Biosens. Bioelectron.* **2015**, *64*, 456–461.

[31] a) X. Yang, M. Feng, J. Xia, F. Zhang, Z. Wang, *J. Electroanal. Chem.* **2020**, *878*, 114669; b) Y. Ma, N. Liu, Z. Xu, J. Wang, X. Luo, *Microchem. J.* **2020**, 161, 105780.

Received: April 19, 2021
Accepted: June 21, 2021
Published online on ■■, ■■

RESEARCH ARTICLE

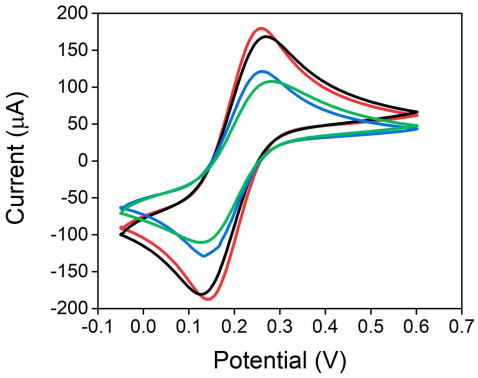

S. N. Topkaya, E. Turunc, A. E. Cetin*